Generalized linear stability of noninertial coating flows over topographical features

Jeffrey M. Davis[a)]
Department of Chemical Engineering, University of Massachusetts, Amherst, Massachusetts 01003

Sandra M. Troian[b)]
Department of Chemical Engineering, Princeton University, Princeton, New Jersey 08544

(Received 4 February 2005; accepted 6 May 2005; published online 24 June 2005)

The transient evolution of perturbations to steady lubrication flow over a topographically patterned surface is investigated via a nonmodal linear stability analysis of the non-normal disturbance operator. In contrast to the capillary ridges that form near moving contact lines, the stationary capillary ridges near trenches or elevations have only stable eigenvalues. Minimal transient amplification of perturbations occurs, regardless of the magnitude or steepness of the topographical features. The absence of transient amplification and the stability of the ridge are explained on physical grounds. By comparison to unstable ridge formation on smooth, flat, and homogeneous surfaces, the lack of closed, recirculating streamlines beneath the capillary ridge is linked to the linear stability. © *2005 American Institute of Physics*. [DOI: 10.1063/1.1945627]

I. INTRODUCTION

Coating flows over surfaces with topographical texture are essential for the fabrication of numerous devices by photolithography, including microelectronic components, integrated circuits, magnetic disks, compact disks, and optical devices. The most effective way to produce the required thin and uniform liquid layers is by spin coating, a method that is widely used in the microelectronics industry for depositing photoresist films. Because of its industrial and technological relevance, liquid film planarization during spin coating has been the focus of numerous theoretical studies.[1–4]

It is quite common for capillary bumps to occur during the coating process, especially in the vicinity of sharp edges on substrate features such as steps, trenches, and mounds. Stillwagon and Larson[5,6] examined the leveling and flow of epoxy and photoresist films over a silicon substrate containing axisymmetric trenches and compared the profilometric measurements to the results from a lubrication model. Finite element solutions by Peurrung and Graves[7] compared favorably to interferometric studies of the film thickness and revealed the source of such phenomena as "pileups" and "wakes" caused by capillary ridges.

Kalliadasis *et al.*[8] recently examined a lubrication model based on Stillwagon and Larson's earlier work for slow, viscous flow over an isolated rectangular trench or mound for a wide range of feature sizes. This analysis revealed that a capillary ridge forms at the entrance to a trench (step-down) and a depression at the base of a mound (step-up), and the ridge amplitude increases with the depth or height of the substrate feature. Mazouchi and Homsy[9] subsequently solved the full Stokes flow equations. For capillary number $\mathrm{Ca} \lesssim 10^{-2}$, the Stokes solution for the film height reduced to the lubrication prediction even for steep features. For $\mathrm{Ca} \approx 1$, however, the amplitude of the capillary bump is diminished, and the liquid film conforms closely to the substrate topography.

On homogeneous surfaces, the presence of a capillary ridge in coating flows driven by either a body force[10–13] or a surface tension gradient[14–18] is linked to the instability of the advancing front to transverse disturbances that evolve into fingers, or rivulets, at the moving contact line. Suppression of the capillary ridge results in a linearly stable film.[12,19] This linkage of the capillary ridge to instability is also supported by results from recent studies of liquid film dynamics on chemically patterned substrates. Liquid confinement to a narrow wetting strip induces a significant transverse curvature of the free surface,[20,21] which suppresses the capillary ridge and fingering instability.[22,23] By contrast, Kalliadasis and Homsy[24] recently found that the stationary capillary ridge near an isolated topographical step-down is asymptotically stable to transverse perturbations. They noted, however, that because the linearized disturbance operator is non–normal, perturbations to the film could possibly grow by orders of magnitude on a transient time scale, thereby exciting nonlinear effects and resulting in an instability. They did not perform a nonmodal analysis or examine the pseudospectra of the disturbance operator.

The present work is a natural extension of this previous study[24] to a nonmodal analysis of the disturbance operator. The initial perturbations localized near the capillary ridge, which experience the largest amplification over various time intervals, are determined, and the evolution of these optimal perturbations is investigated. The analysis is also extended to topographical features of finite width ("mounds" and "trenches"). Despite the association of a capillary ridge with the fingering instability in coating flows over flat surfaces, this result does not hold for flow over topographical features.

[a)]Electronic mail: jmdavis@ecs.umass.edu URL: http://www.ecs.umass.edu/che/faculty/davis.html
[b)]Electronic mail: stroian@princeton.edu URL: http://www.princeton.edu/~stroian/

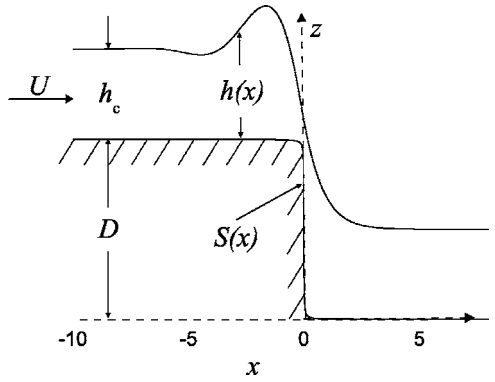

FIG. 1. Sketch of flow over a topographical step-down. The fluid flows from left to right with characteristic velocity U and thickness h_c away from the topographical feature. This topographical step-down has the profile $S(x) = D[0.5 - (1/\pi)\arctan(x/\delta)]$, where D is the feature depth and δ the wall steepness. The orthogonal coordinate system (x,z) has its origin on the step-down.

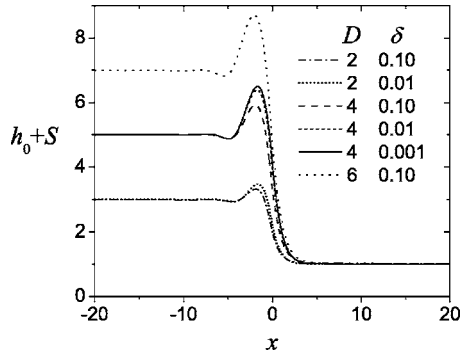

FIG. 2. Numerical solution of Eq. (1) for several values of the step height D and steepness δ.

It is shown in Sec. VI that the stability of both types of capillary ridges can alternatively be inferred from the streamlines of the flow. Instability of the base state is linked to the existence of closed streamlines (in the reference frame that renders the ridge stationary), which indicates the presence of recirculation. This criterion distinguishes between the instability of capillary ridges in films with advancing[10,11,14] or receeding contact lines[25,26] and the stability of stationary capillary ridges induced by topographical features, and also links the instability to the internal flow pattern of the film.

II. FORMULATION OF BASE STATE ANALYSIS

Consider the motion of a thin liquid film driven by a body force over a topographically patterned substrate. The fluid has density ρ, viscosity μ, and surface tension γ. The film has characteristic velocity U and thickness h_c far away from the topographical feature. For flow driven by gravity, the characteristic velocity is given by $U=\rho g \sin(\theta) h_c^2/\mu$, with θ the inclination angle of the substrate from horizontal. For centrifugally driven flow, the characteristic velocity is $U=h_c^2\rho\omega^2 r/\mu$. The angular velocity of rotation is denoted by ω, and r is the radial coordinate measured from the axis of rotation. If the characteristic length of the surface feature is much less than r, then the velocity of the fluid is nearly constant in the vicinity of the feature.[6] This approximation is implicitly assumed in the derivation that follows. A schematic diagram of the flow being considered is shown in Fig. 1.

Within the lubrication approximation, for flow in the $\hat{\boldsymbol{x}}$ direction that is driven by an external body force, the dimensionless equation governing the evolution of the film thickness $h(x,y,t)$ is given by[8]

$$\frac{\partial h}{\partial t} + (h^3)_x + \boldsymbol{\nabla}\cdot[h^3\boldsymbol{\nabla}\nabla^2(h+S)] = 0, \tag{1}$$

where $S(x) = D[1/2 - 1/\pi \tan^{-1}(x/\delta)]$ is the surface profile of the solid substrate for an isolated step-down. [This equation and the analysis that follows can easily be generalized to flows subject to an external shear stress τ, where $U = \tau h/(2\mu)$; the term h_x^3 is then replaced by h_x^2.] The height of the step-down is determined by the constant D, and the steepness is controlled by δ. The scaling used to nondimensionalize h, D, and S is h_c. The dynamic capillary length,[10] $l = h_c \mathrm{Ca}^{-1/3}$, with $\mathrm{Ca} = \mu U/\gamma$ the capillary number, is used to nondimensionalize x and δ. Typical one-dimensional, steady-state base flow solutions $h_0(x)$ to this equation, subject to the conditions $h_0(x) \to 1$ as $x \to \pm\infty$, are shown in Fig. 2. The nonhomogeneous profiles, whose capillary ridge amplitude increases with feature depth and wall steepness, are in agreement with the previous studies.[8,24]

The dimensionless velocity profile in the streamwise direction, from which Eq. (1) is derived, is

$$u(x,z) = \frac{1}{h_0^3}\left(h_0 z - \frac{z^2}{2}\right). \tag{2}$$

The stream function ψ, defined by $u = \partial\psi/\partial z$, therefore has the simple form

$$\psi = \frac{1}{h_0^3}\left(\frac{h_0 z^2}{2} - \frac{z^3}{6}\right). \tag{3}$$

The vertical velocity $w(x,z)$ can be obtained from $w = -\partial\psi/\partial x$. Streamlines are shown for flow over topographical features with finite width in Sec. V.

III. FORMULATION OF LINEAR STABILITY ANALYSIS

The stability of Eq. (1) to disturbances in the transverse direction is analyzed by letting $h(x,y,t) = h_0(x) + \epsilon G(x,t)\exp(iqy)$, with $\epsilon \ll 1$ and q the wavenumber of the disturbance. Substituting for h in Eq. (1) and linearizing with respect to G, the resulting equation for the evolution of perturbations is

$$\frac{\partial G}{\partial t} = -\frac{\partial}{\partial x}\left[h_0^3\left(\frac{\partial^3 G}{\partial x^3} - q^2\frac{\partial G}{\partial x}\right) + 3\frac{1-h_0^3}{h_0}G\right] - 3\frac{\partial}{\partial x}(h_0^2 G) + h_0^3\left(q^2\frac{\partial^2 G}{\partial x^2} - q^4 G\right). \tag{4}$$

Because the discrete spectrum does not exist above a critical wavelength,[24] the boundary conditions for a modal stability analysis are that G is bounded as $x \to \pm\infty$ so that the continuous eigenvectors can be determined. For a nonmodal analysis of the behavior of perturbations to the capillary ridge, how-

ever, it is most appropriate to focus on disturbances that are localized near this ridge. The decay boundary conditions $G \to 0$ as $x \to \pm\infty$ can then be imposed. The influence of these boundary conditions was checked by successively increasing the domain size. A negligible influence on the transient amplification of perturbations to the ridge was found as the domain length was increased. A more general condition that G is bounded was also used in some of the numerical works, but this boundary condition has only a minor effect on the transient amplification of perturbations and does not affect the results near the capillary ridge.

The linearized equation governing the evolution of perturbations to the flow, Eq. (4), can be discretized via a centered difference scheme and can be expressed as

$$\frac{d\boldsymbol{v}}{dt} = \mathbf{A}\boldsymbol{v}, \tag{5}$$

where $\boldsymbol{v}(t)$ is the discrete representation of $G(x,t)$. For all driven films with spatially nonuniform base states, the disturbance operator $\mathbf{A}$ is non-normal, so traditional eigenvalue analysis formally predicts only the asymptotic $t \to \infty$ behavior of solutions to the linearized equation.[16–18,27] Significant perturbation amplification could occur on transient time scales and possibly induce nonlinear effects, which might lead to an observed instability even if the spectrum of $\mathbf{A}$ is confined to the stable half plane.

In generalized linear stability theory, which captures the transient behavior of solutions to Eq. (5), the propagator is most conveniently analyzed in the Euclidean, or l_2, norm. The spectral norm of the propagator, $\|\exp(t\mathbf{A})\|_2$, which represents the maximum amplification of any possible initial condition for Eq. (4), is equivalent to the leading singular value found from the singular value decomposition (SVD) of the propagator, which is given by[27]

$$\exp(t\mathbf{A}) = \mathbf{U}\boldsymbol{\Sigma}\mathbf{V}^{\dagger}, \tag{6}$$

where † denotes the Hermitian transpose. With this inner product that generates the Euclidean norm for the vector space, a complete set of orthogonal perturbations (the columns of $\mathbf{V}$) can be found and ordered by growth over time t from the SVD. The columns of $\mathbf{U}$ are the corresponding evolved states at time t, and the magnitude of each state is given by the associated element of the diagonal matrix $\boldsymbol{\Sigma}$. The associated vector norm is then equivalent to the usual definition of length of a vector:

$$\|\boldsymbol{v}\|_2 = (\boldsymbol{v}^{\dagger}\boldsymbol{v})^{1/2} = \left(\sum_{i=1}^{n} |v_i|^2\right)^{1/2}, \tag{7}$$

where v_i are the n elements comprising $\boldsymbol{v}$.

For perturbations to the free surface flow (which are square integrable), the relevant norm is the L_2 norm of the evolving perturbation, which is given by

$$\|G\| = \left(\int_{-\infty}^{\infty} |G|^2 dx\right)^{1/2}. \tag{8}$$

For perturbations without compact support, the relevant measure is the norm per unit length. In practice, since the base flow and perturbations must be determined numerically, a discrete representation of this norm must be employed. If the grid spacing is fine and uniform, the l_2 norm provides a simple, discrete approximation of the required numerical integral. For nonuniform grids, however, this discrete norm does not measure the quantity of interest, since the perturbation values in the most dense regions of the mesh dominate the l_2 norm. In order to overcome this difficulty while retaining the benefits of this generalized linear stability analysis, new variables can be introduced such that the analysis still proceeds in the Euclidean norm.[27]

Introduce a positive definite Hermitian form $\mathbf{M}$ such that the inner product is defined by

$$(\boldsymbol{v},\boldsymbol{v}) \equiv \boldsymbol{v}^{\dagger}\mathbf{M}\boldsymbol{v}. \tag{9}$$

In the simplest case, $\mathbf{M}$ would be a diagonal matrix with entries $M_{ii} = \Delta x_i$, where Δx_i is the grid spacing between node points i and $i+1$. The associated vector norm is $\|\boldsymbol{v}\|_{2^*} \equiv (\boldsymbol{v}^{\dagger}\mathbf{M}\boldsymbol{v})^{1/2}$, where 2^* indicates the discrete analog of the L_2 norm. Defining the new variables $\boldsymbol{u} = \mathbf{M}^{1/2}\boldsymbol{v}$, the dynamical system in Eq. (5) becomes

$$\frac{d\boldsymbol{u}}{dt} = \mathbf{D}\boldsymbol{u}, \tag{10}$$

with $\mathbf{D} = \mathbf{M}^{1/2}\mathbf{A}\mathbf{M}^{-1/2}$ and $\|\boldsymbol{u}\|_2 = (\boldsymbol{u}^{\dagger}\boldsymbol{u})^{1/2} = \|\boldsymbol{v}\|_{2^*}$. The stability analysis can then be conducted using these new variables, since the l_2 norms of $\boldsymbol{u}$ and $\mathbf{D}$ are the discrete representations of the L_2 norms of $\boldsymbol{G}$ and $\mathbf{A}$, respectively. Using such a transformation of variables yields results from the transient analysis that are mesh independent (and that are identical to results for a very dense, uniform mesh), as required.

Alternatively, the temporal evolution of specific initial conditions can be determined by numerically integrating Eq. (4) forward in time, although the initial disturbance must be arbitrarily selected. The most rapidly growing perturbation and its amplification over a specified time interval t_f can be determined from this approach, however, through the application of a power method to Eq. (4), which is equivalent to solving a series of initial value problems.[28] A first guess for the disturbance is integrated forward in time from $t=0$ to $t=t_f$. This result is then integrated backward in time from $t=t_f$ to $t=0$ with the adjoint equation associated with Eq. (4) to find the new initial condition. This procedure is repeated until convergence to the perturbation with maximum amplification is attained. Results based on a finite element discretization of Eq. (4) and an implicit time step based on Gear's method agree with those reported below, which further confirms the validity of the numerical methods.

IV. RESULTS: STEP-DOWN

A. Modal analysis

Assuming exponential time dependence for G in Eq. (4) gives rise to the discretized eigenvalue problem $\beta\boldsymbol{u} = \mathbf{D}\boldsymbol{u}$, or equivalently $\beta\boldsymbol{v} = \mathbf{A}\boldsymbol{v}$, since the eigenvalues β are independent of the choice of norm. The eigenvalues of $\mathbf{D}$ and the SVD of $\exp(t\mathbf{D})$ were calculated using MATLAB5.3, and the accuracy of the numerical computations was determined by mesh refinement. In addition, the numerically determined ei-

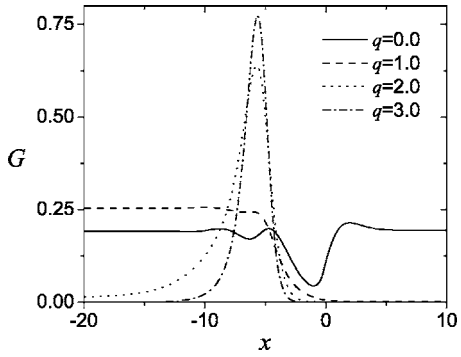

FIG. 3. The least stable eigenvector G for the base flow with $D=6$ and $\delta=0.10$ for several wavenumbers q. The eigenvectors are normalized such that $\int_{x=-20}^{x=10} G^2 dx = 1$.

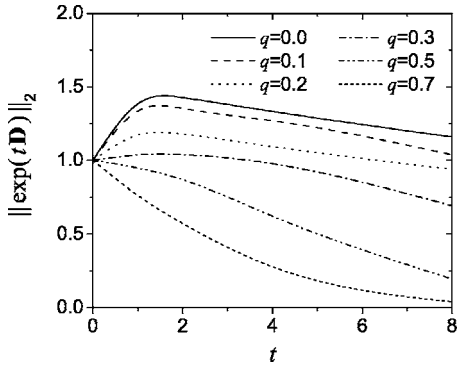

FIG. 4. The maximum amplification ratio of a disturbance applied to the film at time $t=0$ for the base flow with $D=6$, $\delta=0.10$, and several wavenumbers q.

genvalues for the continuous spectrum were found to be in excellent agreement with the analytical relation[24] $\beta=-q^4$ for the least stable mode. The leading eigenvector for the base flow with $D=6$ and $\delta=0.10$ is plotted in Fig. 3 for several wavenumbers q. The eigenvector is localized near the capillary ridge only for sufficiently large q and evolves into the leading continuous eigenfunction for small q. It is interesting to note that the discrete eigenfunctions are centered near the depression in the base flow upstream of the capillary ridge rather than at the ridge itself. Eigenvectors for other base flows are qualitatively similar, although the discrete eigenfunctions move closer to the capillary ridge when the amplitude of this ridge is smaller.

B. Transient growth analysis

Away from the topographical step-down, the base flow is given by the constant solution $h_0=1$, so the linearized disturbance operator for these isolated regions is normal. Since a flat film consequently has a complete set of orthogonal eigenvectors and is linearly stable without inertia,[29] amplification of disturbances far from the capillary ridge cannot occur. The investigation of disturbance amplification is therefore focused on disturbances that are localized near the capillary ridge and decay as $x \to \pm\infty$. The transient evolution of such disturbances is investigated for numerous values of the parameters D and δ, including those corresponding to each base flow shown in Fig. 2, by computing the temporal evolution of $\|\exp(t\mathbf{D})\|$. The maximum amplification of any (infinitesimal) disturbance applied to the system is plotted in Fig. 4 for $D=6$ and $\delta=0.10$ and in Fig. 5 for $D=2$ and $\delta=0.01$. The transient amplification is largest for the smallest wavenumbers, but the maximum amplification ratio is less than 2 for any possible initial disturbance to any of the base states considered. Interestingly, the maximum amplification of localized disturbances is only very weakly affected by the height of the step, D, and the steepness of the topographical feature, δ. These results indicate that although the base state has pronounced spatial variation in the vicinity of the topographical feature (i.e., the induced capillary ridge), the governing disturbance operator is only weakly non-normal, and this weak non-normality has a minimal effect on the temporal evolution of disturbances to the system. This limited non-normality is expected because the discrete spectrum vanishes for small wavenumbers, indicating that the capillary ridge is only weakly affected by long-wavelength transverse perturbations. Instabilities can still occur as the liquid-solid contact line first passes over the topographical features (or even homogeneous regions of the substrate), but examination of such cases is beyond the scope of the current work. The evolution of the unperturbed free-surface profile as the contact line moves over such topographical features has recently been determined within the Stokes flow regime by Gramlich *et al.*[30]

The robust stability and minimal transient amplification of disturbances to the film profile are in complete agreement with recent results from the work of Bielarz and Kalliadasis.[31] These authors studied the nonlinear evolution of particular disturbances applied to time-dependent, thin film coating flows over topography. Even for perturbations that varied sinusoidally in the transverse direction, the ratio of the amplitude of the evolved perturbations to their initial amplitude was less than unity at any time. For the optimal disturbances considered in the present work, which (based on the linear theory) experience the largest amplification of any possible perturbation, the maximum amplification ratio in the 2-norm, $\|\exp(t\mathbf{D})\|_2$, increases only slightly above unity be-

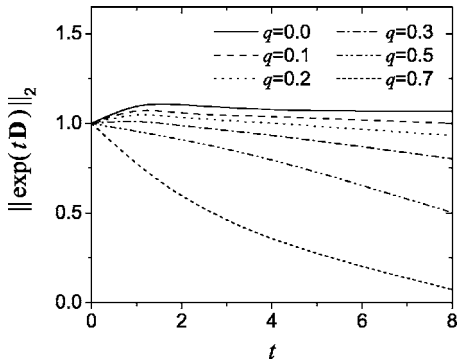

FIG. 5. The maximum amplification ratio of a disturbance applied to the film at time $t=0$ for the base flow with $D=2$, $\delta=0.01$, and several wavenumbers q.

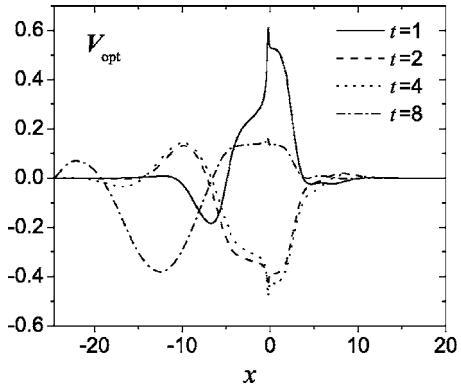

FIG. 6. The optimal disturbances that undergo maximum amplification over the time interval t for the base flow with $D=6$ and $\delta=0.10$ for $q=0.10$.

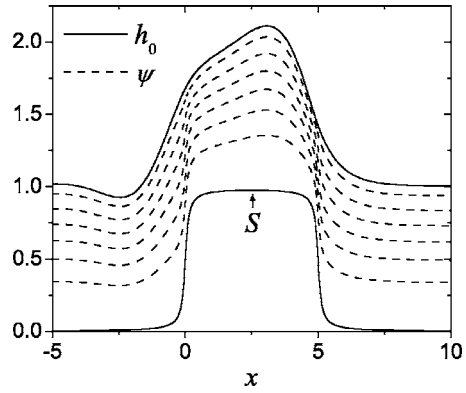

FIG. 8. Base state profile and streamlines for flow over a mound. The parameters are $D=1$, $\delta=0.1$, and $w=5$. The magnitude of the stream function ψ for the dashed lines begins at 0.30 and sequentially decreases by 0.05.

fore decaying to zero for $t \gg 1$. In the ∞-norm, which characterizes the amplitude rather than the magnitude, even these optimal perturbations decay monotonically.

C. Optimal perturbations

The optimal perturbation $\boldsymbol{V}_{\text{opt}}$ is defined as the disturbance of transverse wavenumber q, applied to the film at $t=0$, that undergoes the maximum possible amplification of any disturbance over the time interval t and is given by the first column of the matrix $\mathbf{V}$. The corresponding evolved state $\boldsymbol{U}_{\text{opt}}$ is the (normalized) shape into which $\boldsymbol{V}_{\text{opt}}$ evolves after time t, i.e., from Eq. (6), $\exp(t\mathbf{D})\boldsymbol{V}_{\text{opt}}=\sigma_{\max}\boldsymbol{U}_{\text{opt}}$, with $\sigma_{\max}=\|\exp(t\mathbf{D})\|$. The amplification plotted in Figs. 4 and 5 is experienced by $\boldsymbol{V}_{\text{opt}}(t,q)$, while suboptimal disturbances will experience even less amplification than those presented here. Further details on optimal perturbations are given in Refs. 17 and 27.

The optimal perturbations to the film and the corresponding evolved states after a time interval t, found from a singular value decomposition of $\exp(t\mathbf{D})$, are plotted in Figs. 6 and 7 for $D=6$ and $\delta=0.10$ for $q=0.10$. Other base states and small wavenumbers yield similar perturbations and evolved states. The optimal excitations that undergo the maximum amplification at short times are focused at the capillary ridge but do not even double in magnitude before they begin to decay, as evident from Fig. 4. The optimal disturbances for later times also have a structure near the beginning of the computational domain, since they are convected further along the film during the time interval considered. Because the magnitude and duration of amplification of disturbances as they pass through the capillary ridge are very small, the evolved states become localized oscillations (due to the imposition of decay boundary conditions at the ends of the computational domain) that decay spatially and temporally.

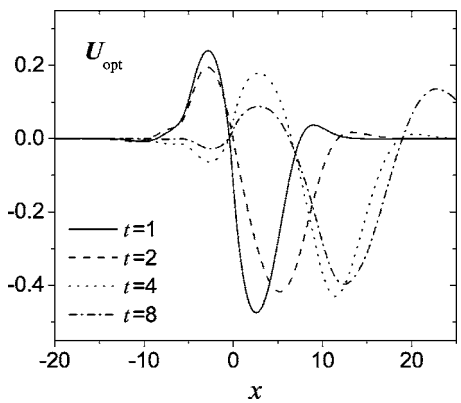

FIG. 7. The evolved states after time t corresponding to the disturbances in Fig. 6.

V. FINITE FEATURES

The stability of flow over finite features was also investigated. A highly localized surface elevation, or mound, can be described by the surface profile

$$S_{\text{mound}}(x) = \frac{D}{\pi}\left[\tan^{-1}\left(\frac{x}{\delta}\right) - \tan^{-1}\left(\frac{x-w}{\delta}\right)\right], \tag{11}$$

where w is the dimensionless width of the feature, while a localized surface indentation, or trench, is described by

$$S_{\text{trench}}(x) = D - S_{\text{mound}}(x). \tag{12}$$

The base state profiles $h_0(x)$ and streamlines $\psi(x)$ for flow over a mound and trench are shown in Figs. 8 and 9, respec-

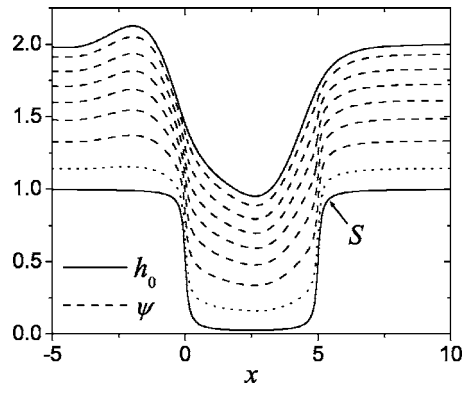

FIG. 9. Base state profile and streamlines for flow over a trench. The parameters are $D=1$, $\delta=0.1$, and $w=5$. The magnitude of the stream function ψ for the dashed lines begins at 0.30 and sequentially decreases by 0.05, while the value for the dotted line is 0.01.

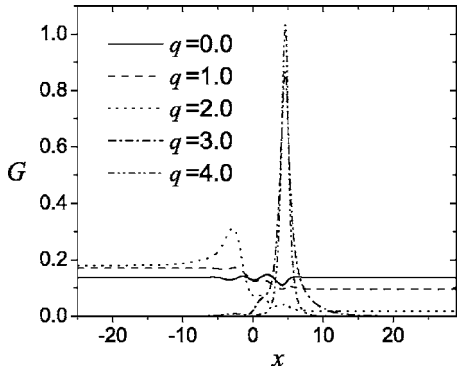

FIG. 10. The least stable eigenvector G for five wavenumbers q for flow over a mound with $D=1.0$, $\delta=0.1$, and $w=5$. The eigenvectors for $q=0.0$, 1.0, and 2.0 are from the continuous spectrum and asymptote to finite values as $x\rightarrow\pm\infty$, while the eigenvectors for $q=3.0$ and 4.0 are discrete and decay as $x\rightarrow\pm\infty$. The eigenvectors are normalized such that $\int_{x=-25}^{x=30}G^2dx=1$.

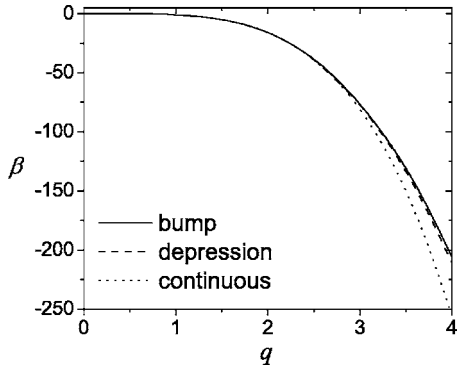

FIG. 12. Dispersion curves $\beta(q)$ for flow over a mound or trench. There is a transition from continuous to discrete modes for $q_c\approx2.45$ for the mound and $q_c\approx2.8$ for the trench. The continuous spectrum $\beta=-q^4$ is shown for comparison.

tively, for $D=1$, $\delta=0.1$, and $w=5$. Profiles for other parameters can be found in Ref. 8, and results from the analysis of film profiles for different regions in parameter space are analogous to those discussed below. The stability analysis for flow over finite features proceeds as in Sec. III for flow over an isolated step-down. Since the coefficients of the linearized disturbance evolution equation depend only on $h_0(x)$ and q [and not $S(x)$], Eq. (4) is valid for arbitrary topography. The least stable eigenvectors for several wavenumbers q are shown in Fig. 10 for flow over a mound and in Fig. 11 for flow over a trench. Although the shape of the eigenvectors differs somewhat from that found in Fig. 3 for the isolated step-down, the general results are similar. As shown in Fig. 12, the dispersion curves differ only slightly from those for flow over an isolated step-down.[24] There is a critical wavenumber q_{crit} below which the discrete spectrum vanishes. In these studies, it was found that $q_c\approx2.45$ for an isolated mound and 2.8 for an isolated trench. Above this wavenumber, the decay rates for the discrete modes are slightly smaller than those for the continuous modes that are given by $\beta=-q^4$. Also, for a given q, disturbances to flow over the mound decay slightly slower than disturbances to flow over the trench.

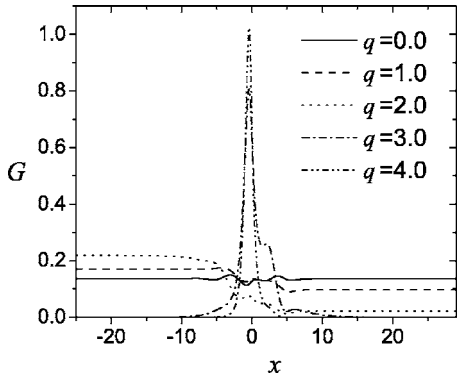

FIG. 11. The least stable eigenvector G for five wavenumbers q for flow over a trench with $D=1$, $\delta=0.1$, and $w=5$. The eigenvectors for $q=0.0$, 1.0, and 2.0 are from the continuous spectrum and are asymptote to finite values as $x\rightarrow\pm\infty$, while the eigenvectors for $q=3.0$ and 4.0 are discrete and decay as $x\rightarrow\pm\infty$. The eigenvectors are normalized such that $\int_{x=-25}^{x=30}G^2dx=1$.

The transient evolution of disturbances to the flow over finite features was also investigated by computing $\|\exp(t\mathbf{D})\|$ vs t for $\mathbf{D}$ given by Eq. (10). As expected from the results for flow over an isolated step-down in Sec. IV B, essentially no transient amplification of perturbations occurs, so the results are not shown here. These results from the analysis of flow over finite topographical features indicate that, as for flow over an isolated step-down, the stable continuous modes associated with capillary waves dominate the evolution of long-wavelength disturbances to the film.

VI. COMPARISON TO NONINERTIAL COATING FLOWS ON SPATIALLY UNIFORM SUBSTRATES

For coating flows driven to spread across a uniform surface by an external body force, the governing evolution equation (that additionally allows for slip at the solid-liquid interface) corresponding to Eq. (1) is[13]

$$h_t+(h^3+\alpha h)_x+\nabla\cdot[(h^3+\alpha h)\nabla(\nabla^2h-N_Dh)]=0, \tag{13}$$

where $N_D=(3\ \mathrm{Ca})^{1/3}\cot(\theta)$ is a dimensionless parameter (denoted D in Ref. 13) that indicates the relative effects of hydrostatic pressure to the body force in the direction of flow, with θ being the angle of inclination of the substrate from horizontal. The dimensionless slip coefficient is denoted α. In a reference frame that moves with the driven spreading film (and thus renders the film profile stationary), the unperturbed base state $h_0(x)$ is determined from

$$h_{0xxx}=1-\frac{1+\alpha}{h_0^2+\alpha}+N_Dh_{0x}. \tag{14}$$

The dimensionless velocity profile in the streamwise direction, from which Eq. (13) is derived, is

$$u(x,z)=\left(-\frac{3}{2}z^2+3hz+\alpha\right)\left(\frac{1+\alpha}{h^2+\alpha}\right)-(1+\alpha), \tag{15}$$

where z is the coordinate normal to the substrate. The stream function $\psi[h_0(x),z]$ is then

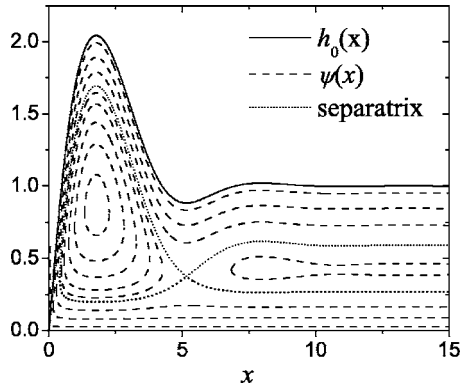

FIG. 13. Base state profile and streamlines near the advancing contact line of a thin liquid film spreading in the $-\hat{x}$ direction under the influence of a body force as determined from Eq. (14) for parameter values $\alpha=0.001$, $D=0$, and $h_{0x}(0)=2$. The film is sufficiently thin that hydrostatic pressure is negligible, and a pronounced capillary ridge develops near the advancing contact line. Note the recirculating flow beneath the ridge. The streamline shown as a solid line is a separatrix, which passes through the stagnation point below the local minimum in the free surface behind the capillary ridge.

$$\psi=\frac{1+\alpha}{h_0^2+\alpha}\left[\frac{1}{2}z^3-\frac{3}{2}h_0z^2-\alpha z\right]+(1+\alpha)z. \tag{16}$$

Plots of the base state profile and streamlines are shown in Figs. 13 and 14. The film profile in Fig. 13 is linearly unstable to transverse disturbances, while the profile in Fig. 14, which lacks a capillary ridge altogether, is perfectly stable. Although not shown, the instability assumes the form of numerous parallel rivulets at the advancing front that result from lateral breakup of the traveling ridge.

The strong stability and lack of transient growth exhibited by capillary ridges induced by topographical features are strikingly different than the behaviors exhibited by capillary ridges that form in driven spreading films. Comparison between these two classes of flows reveals two key distinctions in the response to transverse perturbations. In particular, while the spatially nonuniform base states for thin film flows

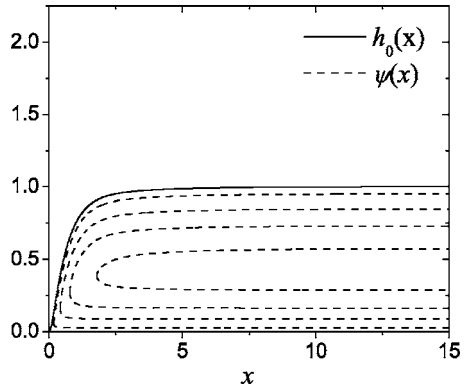

FIG. 14. Base state profile and streamlines near the advancing contact line of a thin liquid film spreading in the $-\hat{x}$ direction under the influence of a body force as determined from Eq. (14) for parameter values $\alpha=0.01$, $D=5$, and $h_{0x}(0)=0.10$. The film is sufficiently thick that hydrostatic pressure prevents the formation of a capillary ridge near the advancing contact line. The absence of recirculating streamlines is similar to the case of steady flow over topographical features discussed earlier, in which the flow is similarly stable.

produce non-normal disturbance operators, the presence of a moving contact line, which distinguishes driven spreading films from the steady flows considered earlier, is primarily responsible for appreciable transient growth of perturbations. Recent nonmodal stability analyses of driven spreading films[13,15–18] have demonstrated that disturbances to the contact line region undergo the largest amount of amplification and that the optimal disturbances (the analog of $\boldsymbol{V}_{\mathrm{opt}}$ in the present work) are sharply peaked at the contact line, thereby confirming an earlier interpretation of contact lines as noise amplifiers.[12] For steady flow over topographical features, there are no moving contact lines, so significant transient amplification of disturbances should not be expected and does not occur.

Furthermore, the streamline patterns provide a more general method for categorizing the stability of capillary ridges and spatially nonuniform thin film flows with respect to the spanwise disturbances responsible for fingering instabilities. This streamline criterion also links the instability to the velocity field in the film. The existence of closed streamlines, which indicate a recirculating flow, implies that the film is linearly unstable. As shown in Fig. 13, such closed streamlines appear in driven spreading films in which there are no stabilizing forces to suppress the formation of a capillary ridge. Streamlines in lubrication models of films driven by surface tension gradients[15] and Stokes flow solutions of flows along an inclined plane[32] are similar. By contrast, the absence of closed streamlines (in a reference frame corresponding to a stationary ridge or liquid front) is strongly linked to film stability. These stable flows correspond to driven spreading films with appreciable hydrostatic pressure or gravitational drainage, in which ridges do not form, and steady flows over topography, which have capillary ridges.

While a formal proof of this criterion for instability based on the structure of the linear operator remains a topic for future study, there are important qualitative differences between capillary ridges that form due to surface heterogeneity and those at moving contact lines. The fingering instability of driven liquid films is a *contact line* instability that also requires significant curvature of the capillary ridge (or, equivalently, the corresponding recirculating flow beneath the ridge). In films with driven contact lines, the capillary ridge is a manifestation of the competition between viscous effects at the solid substrate, which retard the flow, and the surface shear stress or body force that drives the flow. The velocity field corresponding to the streamlines shown in Fig. 13 requires an appropriate pressure gradients, which in such thin films must be supplied by a change in the interfacial curvature. For such flows, the transient amplification occurs as the film adjusts to disturbances at the moving contact line. If a thin precursor film is used as the contact line model, disturbances on the precursor film decay very slowly[14] (as $-h_c^3q^4$) because the film is extremely thin in these regions, and these disturbances therefore essentially retain their initial magnitude as they are convected (in a moving reference frame) to the contact line, at which point nonmodal amplification occurs.[12,15] For the steady-state flow over topographically patterned substrates considered presently, the capillary ridge is stationary and forms in response to a capillary pres-

sure gradient imposed by the surface patterning (surface tension smooths out the liquid profile near the change in surface height), and the (dimensionless) film is relatively thick away from this ridge. Disturbances ahead of or behind the ridge therefore decay more quickly than disturbances to a thin precursor film. Disturbances ahead of the ridge are convected away from it by the flow, and disturbances upstream of the ridge are simply convected through the ridge. Because there is no contact line in steady-state coating flow over surfaces with topographical texture, minimal transient amplification occurs.

The linear stability of the ridges that form in steady flow over topography is also expected because, in contrast to spreading films, there are no closed streamlines and therefore no recirculating flow. Unless the capillary ridge has extremely high curvature such that the Rayleigh instability may be important (in which case the assumptions leading to the lubrication approximation may not hold), a stationary capillary ridge induced by topographical features should be stable. The motion of the contact line associated with the capillary ridge in coating flows (or in dewetting), and not simply the presence of the capillary ridge, is necessary for the development of the well-known fingering instability. In these driven spreading films, disturbances to the capillary ridge are convected along with the film and therefore remain localized at the capillary ridge as they grow or decay. For the stationary capillary ridges that form in flow over topographical features, disturbances of low wavenumbers do not localize at the ridge but are instead convected through it by the flow. Disturbances of higher wavenumbers (for which the discrete spectrum exists), which do localize near the capillary ridge, are highly oscillatory in the transverse direction and hence rapidly damped by surface tension.

VII. CONCLUSION

Although the formation of a capillary ridge at the moving front is linked to the development of a fingering instability in coating flows over flat surfaces, the stationary capillary ridges that form in response to topographical features are stable to transverse perturbations. The stability of both types of capillary ridges can instead be inferred from the streamlines of the flow. The existence of closed streamlines in the reference frame that renders a capillary ridge stationary, which indicates the presence of recirculation, is associated with the instability of the ridge. The lack of closed, recirculating streamlines beneath capillary ridges that are induced by topographical features is directly linked to the linear stability of the ridges. Furthermore, regardless of the amplitude or steepness of the topographical feature, minimal transient amplification of perturbations is found to occur, indicating that the linear stability predictions for noninertial coating flows over topography should be physically determinant.

ACKNOWLEDGMENTS

This work was supported by the NASA Microgravity Fluid Physics Program, the U.S. Army TACOM-ARDEC, and the Princeton Research Institute for the Science of Materials. J.M.D. wishes to thank the Air Force Office of Scientific Research for a NDSEG Fellowship and Princeton University for the G. Van Ness Lothrop Fellowship in Engineering. S.M.T. kindly acknowledges the warm hospitality and generous financial support received through the Moore Distinguished Scholar Program at the California Institute of Technology.

[1] A. G. Emslie, F. T. Bonner, and L. G. Peck, "Flow of a viscous liquid on a rotating disk," J. Appl. Phys. **29**, 858 (1958).
[2] A. Acrivos, M. J. Shah, and E. E. Petersen, "On the flow of a non-Newtonian liquid on a rotating disk," J. Appl. Phys. **31**, 963 (1960).
[3] P. C. Sukanek, "A model for spin coating with topography," J. Electrochem. Soc. **136**, 3019 (1989).
[4] W. Brodkorb, J. M. Köhler, and O. Ritzel, "A hydrodynamical model for the spin-coated substrate topography," Exp. Tech. Phys. (Berlin) **37**, 519 (1989).
[5] L. E. Stillwagon and R. G. Larson, "Fundamentals of topographic substrate leveling," J. Appl. Phys. **63**, 5251 (1988).
[6] L. E. Stillwagon and R. G. Larson, "Leveling of thin films over uneven substrates during spin coating," Phys. Fluids A **2**, 1937 (1990).
[7] L. M. Peurrung and D. B. Graves, "Spin coating over topography," IEEE Trans. Semicond. Manuf. **6**, 72 (1993).
[8] S. Kalliadasis, C. Bielarz, and G. M. Homsy, "Steady free-surface thin film flows over topography," Phys. Fluids **12**, 1889 (2000).
[9] A. Mazouchi and G. M. Homsy, "Free surface Stokes flow over topography," Phys. Fluids **13**, 2751 (2001).
[10] S. M. Troian, E. Herbolzheimer, S. A. Safran, and J. F. Joanny, "Fingering instabilities of driven spreading films," Europhys. Lett. **10**, 25 (1989).
[11] M. A. Spaid and G. M. Homsy, "Stability of Newtonian and viscoelastic dynamic contact lines," Phys. Fluids **8**, 460 (1996).
[12] A. L. Bertozzi and M. P. Brenner, "Linear stability and transient growth in driven contact lines," Phys. Fluids **9**, 530 (1997).
[13] J. M. Davis and S. M. Troian, "On a generalized approach to the linear stability of spatially nonuniform thin film flows," Phys. Fluids **15**, 1344 (2003).
[14] D. E. Kataoka and S. M. Troian, "A theoretical study of instabilities at the advancing front of thermally driven coating films," J. Colloid Interface Sci. **192**, 350 (1997).
[15] J. M. Davis and S. M. Troian, "Influence of attractive van der Waals interactions on the optimal excitations in thermocapillary driven spreading," Phys. Rev. E **67**, 016308 (2003).
[16] J. M. Davis, B. J. Fischer, and S. M. Troian, "A general approach to the linear stability of thin spreading films," in *Interfacial Fluid Dynamics and Transport Processes*, Lecture Notes in Physics, edited by R. Narayanan (Springer, Heidelberg, 2003), pp. 79–106.
[17] J. M. Davis, "Dynamics and linear stability of thermocapillary spreading films on homogeneous and micropatterned surfaces," Ph.D. thesis, Princeton University, 2003.
[18] J. M. Davis and S. M. Troian, "Influence of boundary slip on the optimal excitations in thermocapillary driven spreading," Phys. Rev. E **70**, 046309 (2004).
[19] D. E. Kataoka and S. M. Troian, "Stabilizing the advancing front of thermally driven coating films," J. Colloid Interface Sci. **203**, 335 (1998).
[20] A. A. Darhuber, S. M. Troian, J. M. Davis, S. M. Miller, and S. Wagner, "Selective dip-coating of chemically micropatterned surfaces," J. Appl. Phys. **88**, 5119 (2000).
[21] J. M. Davis, "Asymptotic analysis of liquid films dip-coated onto chemically micropatterned surfaces," Phys. Fluids **17**, 038101 (2005).
[22] D. E. Kataoka and S. M. Troian, "Patterning liquid flow at the microscopic scale," Nature (London) **402**, 794 (1999).
[23] A. A. Darhuber, J. M. Davis, S. M. Troian, and W. W. Reisner, "Thermocapillary actuation of liquid flow on chemically patterned surfaces," Phys. Fluids **15**, 1295 (2003).
[24] S. Kalliadasis and G. M. Homsy, "Stability of free-surface thin-film flows over topography," J. Fluid Mech. **448**, 387 (2001).
[25] P. G. Lopez, M. J. Miksis, and S. G. Bankoff, "Stability and evolution of a dry spot," Phys. Fluids **13**, 1601 (2001).
[26] A. V. Lyushnin, A. A. Golovin, and L. M. Pismen, "Fingering instability of thin evaporating liquid films," Phys. Rev. E **65**, 021602 (2002).
[27] B. F. Farrell and P. J. Ioannou, "Generalized stability theory. Part 1: Autonomous operators," J. Atmos. Sci. **53**, 2025 (1996).

[28]A. M. Moore and B. F. Farrell, "Rapid perturbation growth on spatially and temporally varying oceanic flows determined using an adjoint method: Application to the Gulf stream," J. Phys. Oceanogr. **23**, 1682 (1993).
[29]T. B. Benjamin, "Wave formation in laminar flow down an inclined plane," J. Fluid Mech. **2**, 554 (1957).
[30]C. M. Gramlich, A. Mazouchi, and G. M. Homsy, "Time-dependent free surface Stokes flow with a moving contact line. II. Flow over wedges and trenches," Phys. Fluids **16**, 1660 (2004).
[31]C. Bielarz and S. Kalliadasis, "Time-dependent free-surface thin film flows over topography," Phys. Fluids **15**, 2512 (2003).
[32]R. Goodwin and G. M. Homsy, "Viscous-flow down a slope in the vicinity of a contact line," Phys. Fluids A **3**, 515 (1991).